A novel form of imperfect contact laws in flexoelectricity

A novel form of imperfect contact laws in flexoelectricity

Michele Serpilli[a,*], Raffaella Rizzoni[b], Reinaldo Rodríguez-Ramos[c], Frédéric Lebon[d], Serge Dumont[e]

[a]*Department of Civil and Building Engineering, and Architecture, Università Politecnica delle Marche, Ancona , Italy*
[b]*Department of Engineering, University of Ferrara, via Saragat 1 44122 Ferrara, Italy*
[c]*Departamento de Matemática, Facultad de Matemática y Computación, Universidad de La Habana, San Lazaro y L, 10400 La Habana, Cuba*
[d]*Aix Marseille Univ, CNRS, Centrale Marseille, LMA, 4 impasse Nikola Tesla 13453 Marseille Cedex 13, France*
[e]*IMAG CNRS UMR 5149, University of Nîmes, 30000 Nîmes, France*

Abstract

Flexoelectric materials exhibit coupling between electric polarization and mechanical strain gradient. At the nano-scale and micro-scale, these materials offer a promising potential for the development of mechanical transducers and energy harvesters. This work proposes a new imperfect interface model simulating the behavior of a thin flexoelectric layer (adhesive) of vanishing thickness, embedded between two flexoelectric media (adherents). The adhesive is assumed to be mechanically compliant and electrically lowly-conducting. The interface model is obtained by using the asymptotic analysis. The contact laws, expressed in terms of the jumps and means values of the displacements, normal derivatives of the displacements, and electric potential across the interface, represent a formal generalization of the soft elastic and piezoelectric interface conditions. A simple application, considering a one-dimensional three-layer composite micro-bar subject to electro-mechanical loads, is developed in order to analytically/numerically assess the asymptotic model. Nonlocal phenomena and end-effects, related to a flexoelectric length-scale parameter, are highlighted. The example illustrates the usefulness of the proposed approach toward the design of thin nano- and microscale devices exploiting the flexoelectric effect.

*Corresponding author

1. Introduction

The conception and use of smart functional materials have undergone major development over the past decades in the fields of civil and mechanical engineering, industrial applications, automation systems, biomedical instruments, and more. Besides, nanotechnologies and system miniaturization offer incredible potential for the conceptual design and the practical realization of radically new smart materials. The main characteristic of smart materials is their ability to change their properties, sense, heal and adapt themselves in response to external stimuli. Smart materials can be subdivided into materials that exhibit either a direct or an indirect coupling. Piezoelectric materials, magnetostrictive ceramics, and flexoelectric materials are a few examples of active materials that exhibit direct/indirect coupling. This means that either the mechanical or the non-mechanical field can serve as an input, while the other as the output. This list cannot be considered comprehensive and exhaustive of all types of functional materials (for more details, see [1]).

Piezoelectric materials exhibit electrical polarization when subjected to a mechanical stress, and conversely deform in response to an applied electric field. They are used in electronic devices as sensors (direct piezoelectric effect), actuators (inverse piezoelectric effect) [2, 3, 4]. Magnetostrictive materials can be magnetized on the application of stress or deform in response to the magnetic field. Due to these capabilities, magnetostrictive structures are excellent candidates to be utilized as sensors and actuators, tuned vibration absorbers, dampers, and energy harvesters [5, 6, 7].

A different effect is flexoelectricity, in which the electrical polarization is induced by a strain gradient. Within crystals, polarization associated with flexoelectricity is originated by the non-uniform displacement of ions under a strain gradient. While piezoelectricity is a linear response of the dielectric polarization to a uniform strain, flexoelectricity is a high-order electromechanical phenomenon coupling strain gradients and electric polarization (see, [8, 9] for a detailed overview).

Apart from hard crystalline materials, flexoelectricity has been observed in soft materials, like biological materials, isotropic elastomers, liquid crystal, and semi-crystalline polymers such as polyvinylidene fluoride, polyurethane and polythiophene films [10, 11, 12, 14, 13, 15]. Being associated with strain gradients, flexoelectricity exhibits an inherent scale effect and it is more predominant at smaller scales (micro-and/or nano-scale). Thus, it is expected to be enhanced in thin layers. Moreover, the progress in nano-technologies has progressively permitted to diminish the size of electromechanical devices and transducers, reaching thicknesses of a few micrometers where gradients are significant [16, 17, 18, 19, 20]. In this case, the flexoelectric effects cannot

be ignored, leading to a drastic performance degradation [21, 22]. This motivates the present work, aimed at studying the behavior of thin flexoelectric interphase within a composite medium, as its thickness vanishes to zero.

Concerning the theoretical aspects of bonded joints modeling, the thin layer between two adjacent bodies can be treated as a two-dimensional surface, called the imperfect interface, on which appropriate transmission conditions are defined. Various interface models for layered composites have been developed throughout the years by means of classical variational tools [23, 24, 25], and more refined mathematical techniques (asymptotic analysis), in linear elasticity [26, 27, 28, 29, 30, 31, 32], and in general multiphysics theories [33, 34], such as continua with microstructure [35, 36], coupled thermoelasticity [37], and piezoelectricity [38, 39, 40]. It is only in recent years that the flexoelectric effect has been incorporated in such theoretical schemes, to: predict the effective properties of heterogeneous flexoelectric multilayer composites, via asymptotic homogenization methods [41, 42, 43]; numerically simulate higher-order weak interface conditions by means of Nitsche's method for complex material architectures, including general multimaterial arrangements [44]; analyze the flexoelectric effect with a highly/weakly interface in distinct piezoelectric materials in [45]. Nevertheless, the previous approaches lack a proper characterization of the transmission conditions for soft or weak interfaces, in terms of the jumps of the flexoelectric state (displacements and electric potential) and its conjugated physical quantities (stresses, electric displacements, and hyper-stresses).

The present paper aims at providing a novel and explicit form of the imperfect interface law for flexoelectric composites by means of an asymptotic analysis. The flexoelectric assembly is constituted by two surrounding media (adherents), connected by an intermediate thin interphase (adhesive), whose thickness depends on a small parameter ε. The elastic, piezoelectric and dielectric coefficients of the intermediate layer are assumed to linearly depend on ε, while the flexoelectric moduli depend on ε^2. The material parameters of the adherents are independent of ε. This allows to characterize the so-called soft interface model. Following the asymptotic approach developed in [33], it is possible to compute the interface law at order 0, defining an original and nontrivial interface model. Lastly, a numerical example has been developed considering a one-dimensional three-layer flexoelectric composite bar, subjected to a tensile load and an assigned electric potential at the free ends. The exact solution of the three-layer configuration is compared with the closed-form solution of a two-layer composite, in which the intermediate adhesive has been replaced by the imperfect contact conditions.

The plan of the paper is the following. Section 2 is a summary of the linear theory for flexoelectric solids, accounting for the weak and strong formula-

tions of the equilibrium problem for a flexoelectric body. The (weak form of the) equilibrium problem of an assemblage incorporating two adherents joined by a soft adhesive is described in Section 3, together with the rescaled governing formulation and asymptotic expansions of the relevant fields. In Section 4, we obtain imperfect contact conditions replacing the behavior of the very thin, soft, flexoelectric adhesive. Here, we discuss the form of the contact conditions comparing them with the classical spring-type interface model and the contact model for a soft piezoelectric interface calculated in [34, 38]. Section 5 is devoted to a one-dimensional example, a flexoelectric three-layer micro-bar. Despite its simplicity, it turns out to be an interesting setting to study the influence of the thin interposed layer on the structural behavior of the structure. Some concluding remarks are addressed in Section 6.

2. Linear theory of flexoelectricity: background

In this section the linear theory for flexoelectric solids is summarized, considering the expression of the constitutive law and the weak and strong formulation of the governing equations. In the sequel, Greek indices range in the set $\{1,2\}$, Latin indices range in the set $\{1,2,3\}$, and the Einstein's summation convention with respect to the repeated indices is adopted. Let us consider a three-dimensional Euclidian space identified by $\mathbb{R}^3$ and such that the three vectors $\mathbf{e_i}$ form an orthonormal basis. We introduce the following notations for the inner and dyadic products: $\mathbf{a}\cdot\mathbf{b} := a_i b_i$, and $\mathbf{a}\otimes\mathbf{b} := (a_i b_j)$, for all vectors $\mathbf{a} = (a_i)$ and $\mathbf{b} = (b_i)$ in $\mathbb{R}^3$.

Considering the case of direct flexoelectricity [46, 47], the electric Gibbs stored energy density $\mathcal{G}$ is given in terms of e_{ij}, $e_{ij,k}$ and E_i, being the linearized strain tensor, the gradient of the linearized strain tensor and the electric field, respectively:

$$\mathcal{G}(e_{ij}, e_{ij,k}, E_i) := \frac{1}{2}c_{ijkl}e_{kl}e_{ij} - p_{ikl}E_i e_{kl} - \mu_{ijkl}E_i e_{jk,l} - \frac{1}{2}\kappa_{ij}E_i E_j,$$

where (c_{ijkl}), (p_{ikl}), (μ_{ijkl}), and (κ_{ij}) represent, respectively, the elasticity tensor, the piezoelectric coupling tensor, the flexoelectric coupling tensor, and the dielectric permittivity tensor and $e_{ij} = \frac{1}{2}(u_{i,j} + u_{j,i})$, $e_{ij,k} = \frac{1}{2}(u_{i,jk} + u_{j,ik})$ and $E_i = -\varphi_{,i}$, with u_i and φ the displacement field and electric potential. We remark that higher order constitutive tensors (i.e. fifth-order and sixth-order tensor) are neglected for the sake of simplicity.

The constitutive law can be derived as follows:

$$\check{\sigma}_{ij} = \frac{\partial \mathcal{G}}{\partial e_{ij}}, \quad \tilde{\sigma}_{ijk} = \frac{\partial \mathcal{G}}{\partial e_{ij,k}}, \quad D_i = -\frac{\partial \mathcal{G}}{\partial E_i},$$

with $(\check{\sigma}_{ij})$, $(\tilde{\sigma}_{ijk})$, and (D_i) denote the Cauchy stress tensor, the hyper-stress tensor and the electric displacement field, respectively. Thus,

$$\begin{aligned} \check{\sigma}_{ij} &= c_{ijkl}e_{kl} - p_{kij}E_k, \\ \tilde{\sigma}_{ijk} &= -\mu_{lijk}E_l, \\ D_i &= p_{ikl}e_{kl} + \mu_{ijkl}e_{jk,l} + \kappa_{ij}E_j. \end{aligned} \tag{1}$$

We note with $\sigma_{ij} := \check{\sigma}_{ij} - \tilde{\sigma}_{ijk,k} = c_{ijkl}e_{kl} - p_{kij}E_k + \mu_{lijk}E_{l,k}$ the so-called physical stress [48]. Using (1), the electric Gibbs energy density takes the following form:

$$\mathcal{G}(e_{ij}, e_{ij,k}, E_i) = \frac{1}{2}\left(\check{\sigma}_{ij}e_{ij} + \tilde{\sigma}_{ijk}e_{ij,k} + D_iE_i\right).$$

Let us consider a material body Ω made of a flexoelectric material, whose constitutive law is defined in (1). The body is subjected to body forces f_i and a volume charge density ρ^e, acting in Ω, and to surface forces g_i, higher-order surface forces r_i and a surface charge source w, applied to the boundary $\Gamma_1 \subset \partial\Omega$. The body is mechanically clamped and electrically short-circuited on $\Gamma_0 \subset \partial\Omega$. The work of external sources is given by

$$L(s) := \int_\Omega \{f_iu_i - \rho^e\varphi\}dx + \int_{\Gamma_1} \{g_iu_i + r_i\partial_n u_i + w\varphi\}d\Gamma,$$

where $s := (\mathbf{u}, \varphi)$ denotes the flexoelectric state. The enthalpy functional Π can now be written in the form:

$$\Pi[s] := \int_\Omega \mathcal{G}(e_{ij}, e_{ij,k}, E_i)dx - L(s).$$

The flexoelectric equilibrium state $s^* = (\mathbf{u}^*, \varphi^*)$ corresponds to the saddle point of the enthalpy potential, fulfilling the variational principle $s^* = \arg\min_{\mathbf{u}\in V(\Omega)} \max_{\varphi\in\Psi(\Omega)} \Pi[s]$, with $V(\Omega) := \{\mathbf{v} \in [H^2(\Omega)]^3 :\ \mathbf{v} = \mathbf{0},\ \partial_n\mathbf{v} = \mathbf{0} \text{ on } \Gamma_0\}$, $\Psi(\Omega) := \{\psi \in H^1(\Omega) :\ \psi = 0 \text{ on } \Gamma_0\}$. The variational formulation of the problem can be derived by enforcing the first variation of the enthalpy functional Π to vanish [47, 49], so that:

$$\begin{cases} \text{Find } s \in \mathcal{V}(\Omega) := V(\Omega) \times \Psi(\Omega), \text{ such that} \\ A(s, r) = L(r), \text{ for all } r := (\mathbf{v}, \psi) \in \mathcal{V}(\Omega), \end{cases} \tag{2}$$

where

$$\begin{aligned} A(s,r) &:= \int_\Omega \left\{\check{\sigma}_{ij}e_{ij}(\mathbf{v}) + \tilde{\sigma}_{ijk}e_{ij,k}(\mathbf{v}) + D_iE_i(\psi)\right\}dx = \\ &= \int_\Omega \{c_{ijkl}e_{kl}(\mathbf{u})e_{ij}(\mathbf{v}) + p_{kij}\left(\varphi_{,k}e_{ij}(\mathbf{v}) - e_{ij}(\mathbf{u})\psi_{,k}\right) + \\ &\quad + \mu_{lijk}(\varphi_{,l}e_{ij,k}(\mathbf{v}) - e_{ij,k}(\mathbf{u})\psi_{,l}) + \kappa_{ij}\varphi_{,i}\psi_{,j}\ \}\,dx. \end{aligned}$$

By virtue of the Gauss-Green's theorem, it is possible to compute the differential form of the equilibrium problem, as follows:

$$-\int_{\Omega}\left\{\sigma_{ij,j}v_i - D_{i,i}\psi\right\}dx + \int_{\partial\Omega}\left\{\sigma_{ij}n_j + \mathcal{D}_l^t(n_l)n_k n_j\tilde{\sigma}_{ijk} - \mathcal{D}_j^t(n_k\tilde{\sigma}_{ijk})\right\}v_i d\Gamma +$$
$$+\int_{\partial\Omega}\left\{\tilde{\sigma}_{ijk}n_j n_k\partial_n v_i - D_i n_i\psi\right\}d\Gamma = L(r),$$

where (n_i) denotes the outer unit normal vector to the boundary $\partial\Omega$, $\mathcal{D}_i^t(\cdot) := (\delta_{ij} - n_i n_j)(\cdot)_{,j}$ and $\partial_n(\cdot) := n_i(\cdot)_{,i}$ are the tangential and normal derivative operators on the boundary, respectively, with δ_{ij} as the Kronecker's symbol. In this formulation, the integral on the boundary edges is neglected. Thus, the governing equations for a flexoelectric material take the following expression:

$$\begin{cases}\sigma_{ij,j} + f_i = 0, \quad D_{i,i} = \rho^e & \text{in } \Omega,\\ T_i := \sigma_{ij}n_j + \mathcal{D}_l^t(n_l)n_k n_j\tilde{\sigma}_{ijk} - \mathcal{D}_j^t(n_k\tilde{\sigma}_{ijk}) = g_i & \text{on } \Gamma_1,\\ R_i := \tilde{\sigma}_{ijk}n_j n_k = r_i & \text{on } \Gamma_1,\\ D_i n_i = -w & \text{on } \Gamma_1,\\ u_i = 0, \quad \partial_n u_i = 0, \quad \varphi = 0 & \text{on } \Gamma_0.\end{cases}$$

T_i and R_i are, respectively, the physical traction vector and the higher-order traction vector. In the presence of a perfect interface S within the material body, the following six continuity conditions must be satisfied:

$$[T_i] = 0, \quad [R_i] = 0, \quad [D_i n_i] = 0, \quad [u_i] = 0, \quad [\partial_n u_i] = 0, \quad [\varphi] = 0,$$

where $[\cdot]$ represents the jump function at the interface S.

3. Statement of the problem for a composite material: asymptotic expansions

Let us define a small parameter $0 < \varepsilon < 1$. We consider the assembly constituted of two solids $\Omega_{\pm}^{\varepsilon} \subset \mathbb{R}^3$, called the adherents, bonded together by an intermediate thin layer $B^{\varepsilon} := S \times (-\frac{\varepsilon}{2}, \frac{\varepsilon}{2})$ of thickness ε, called the adhesive, with cross-section $S \subset \mathbb{R}^2$. In the following B^{ε} and S will be called interphase and interface, respectively. Let $S_{\pm}^{\varepsilon}$ be the plane interfaces between the interphase and the adherents and let $\Omega^{\varepsilon} := \Omega_{+}^{\varepsilon} \cup B^{\varepsilon} \cup \Omega_{-}^{\varepsilon}$ denote the composite system comprising the interphase and the adherents, (cf. Figure 1a). The variational form of the flexoelectric problem defined on the variable

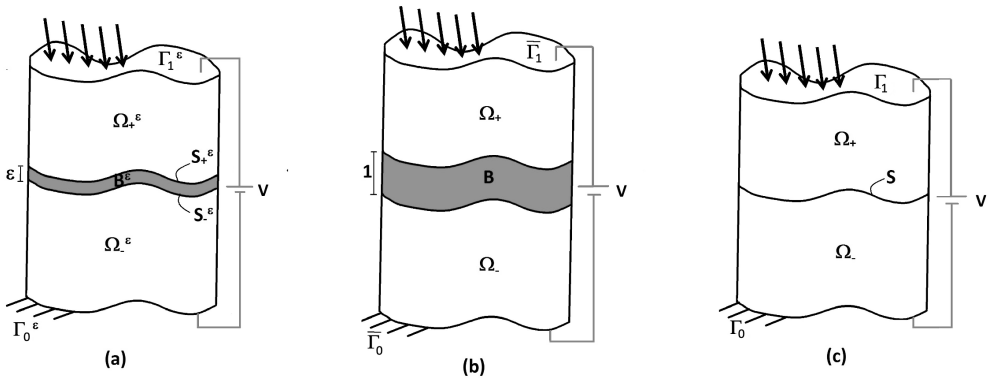

Figure 1: Initial (a), rescaled (b) and limit (c) configurations of the composite.

domain Ω^ε can be derived as follows:

$$\begin{cases} \text{Find } s^\varepsilon \in \mathcal{V}(\Omega^\varepsilon), \ \text{ such that} \\ \bar{A}^\varepsilon_-(s^\varepsilon, r^\varepsilon) + \bar{A}^\varepsilon_+(s^\varepsilon, r^\varepsilon) + \hat{A}^\varepsilon(s^\varepsilon, r^\varepsilon) = L^\varepsilon(r^\varepsilon), \ \text{for all } r^\varepsilon \in \mathcal{V}(\Omega^\varepsilon). \end{cases} \tag{3}$$

In order to study the asymptotic behavior of the solution of problem (3) when ε tends to zero, we rewrite the problem on a fixed domain Ω independent of ε. By using the approach of [50], let us consider the change of coordinate $\pi^\varepsilon : x \in \overline{\Omega} \mapsto x^\varepsilon \in \overline{\Omega}^\varepsilon$ given by

$$\pi^\varepsilon : \begin{cases} \bar{\pi}^\varepsilon(x_1, x_2, x_3) = (x_1, x_2, x_3 \mp \frac{1}{2}(1-\varepsilon)), & \text{for all } x \in \overline{\Omega}_\pm, \\ \hat{\pi}^\varepsilon(x_1, x_2, x_3) = (x_1, x_2, \varepsilon x_3), & \text{for all } x \in \overline{B}, \end{cases}$$

where, after the change of variables, the adherents occupy $\Omega_\pm := \Omega^\varepsilon_\pm \pm \frac{1}{2}(1-\varepsilon)\mathbf{e}_3$ and the interphase $B = \{x \in \mathbb{R}^3 : \ (x_1, x_2) \in S, \ |x_3| < \frac{1}{2}\}$. The sets $S_\pm = \{x \in \mathbb{R}^3 : \ (x_1, x_2) \in S, \ x_3 = \pm\frac{1}{2}\}$ denote the interfaces between B and $\Omega_\pm$ and $\Omega = \Omega_+ \cup \Omega_- \cup B$ is the rescaled configuration of the composite, see Fig. 1b. Lastly, Γ_0 and Γ_1 indicate the images through π^ε of Γ^ε_0 and Γ^ε_1 (cf. Figure 1.b). Consequently, $\frac{\partial}{\partial x^\varepsilon_\alpha} = \frac{\partial}{\partial x_\alpha}$ and $\frac{\partial}{\partial x^\varepsilon_3} = \frac{\partial}{\partial x_3}$ in $\Omega_\pm$, and $\frac{\partial}{\partial x^\varepsilon_\alpha} = \frac{\partial}{\partial x_\alpha}$ and $\frac{\partial}{\partial x^\varepsilon_3} = \frac{1}{\varepsilon}\frac{\partial}{\partial x_3}$ in B. In the sequel, only if necessary, $\bar{s}^\varepsilon = (\bar{\mathbf{u}}^\varepsilon, \bar{\varphi}^\varepsilon)$ and $\hat{s}^\varepsilon = (\hat{\mathbf{u}}^\varepsilon, \hat{\varphi}^\varepsilon)$ will note the restrictions of functions $s^\varepsilon = (\mathbf{u}^\varepsilon, \varphi^\varepsilon)$ to $\Omega_\pm$ and B.

The constitutive coefficients of $\Omega^\varepsilon_\pm$ are assumed to be independent of ε, while the constitutive tensors of B^ε present the following dependences on ε:

$$\hat{c}^\varepsilon_{ijkl} = \varepsilon^q \hat{c}_{ijkl}, \ \hat{p}^\varepsilon_{ijk} = \varepsilon^q \hat{p}_{ijk}, \ \hat{\kappa}^\varepsilon_{ij} = \varepsilon^q \hat{\kappa}_{ij}, \ \hat{\mu}^\varepsilon_{ijkl} = \varepsilon^{q+1} \hat{\mu}_{ijkl}.$$

The choice of the exponent $q+1$ for $\hat{\mu}^\varepsilon_{ijkl}$ can be considered the only suitable assumption to let the flexoelectric behavior appear in the limit model. From

a technical point of view, this exponent is justified by the fact that the flexoelectric coefficients are related to the strain gradient, depending on the second derivatives of the displacement field.

The limit behavior for a soft flexoelectric interface with low conductivity can be characterized by choosing $q = 1$. Finally, the data, unknowns and test functions verify the following scaling assumptions:

$$\begin{array}{llll} s^\varepsilon(x^\varepsilon) = s^\varepsilon(x), & r^\varepsilon(x^\varepsilon) = r(x) & & x \in \Omega, \\ f_i^\varepsilon(x^\varepsilon) = f_i(x), & \rho^{e,\varepsilon}(x^\varepsilon) = \rho^e(x) & & x \in \Omega_\pm, \\ g_i^\varepsilon(x^\varepsilon) = g_i(x), & r_i^\varepsilon(x^\varepsilon) = r_i(x) & w^\varepsilon(x^\varepsilon) = w(x), & x \in \Gamma_1, \end{array}$$

so that $L^\varepsilon(r^\varepsilon) = L(r)$. According to the previous scaling assumptions, problem (3) can be rewritten on a fixed domain Ω independent of ε. Thus, the following rescaled problem is obtained:

$$\left\{ \begin{array}{l} \text{Find } s^\varepsilon \in \mathcal{V}(\Omega), \ \text{ such that} \\ \bar{A}_-(s^\varepsilon, r) + \bar{A}_+(s^\varepsilon, r) + \varepsilon^2 \hat{A}(s^\varepsilon, r) = L(r), \ \text{ for all } r \in \mathcal{V}(\Omega), \end{array} \right. \tag{4}$$

where $\hat{A}(s^\varepsilon, r) := \frac{1}{\varepsilon^2} a_0(s^\varepsilon, r) + \frac{1}{\varepsilon} a_1(s^\varepsilon, r) + a_2(s^\varepsilon, r) + \varepsilon a_3(s^\varepsilon, r)$, with

$$\begin{aligned} a_0(s^\varepsilon, r) := & \int_B \big\{ \hat{c}_{i3j3} u^\varepsilon_{j,3} v_{i,3} + \hat{p}_{3i3}(\varphi^\varepsilon_{,3} v_{i,3} - \psi_{,3} u^\varepsilon_{i,3}) + \hat{\kappa}_{33} \varphi^\varepsilon_{,3} \psi_{,3} + \\ & + \hat{\mu}_{i333}(\varphi^\varepsilon_{,3} v_{i,33} - \psi_{,3} u^\varepsilon_{i,33}) \big\} \, dx, \\ a_1(s^\varepsilon, r) := & \int_B \big\{ \hat{c}_{i3j\alpha}(u^\varepsilon_{j,3} v_{i,\alpha} + u^\varepsilon_{j,\alpha} v_{i,3}) + \hat{p}_{3\alpha i}(\varphi^\varepsilon_{,3} v_{i,\alpha} - \psi_{,3} u^\varepsilon_{i,\alpha}) + \\ & + \hat{p}_{\alpha 3 i}(\varphi^\varepsilon_{,\alpha} v_{i,3} - \psi_{,\alpha} u^\varepsilon_{i,3}) + \hat{\kappa}_{\alpha 3}(\varphi^\varepsilon_{,3} \psi_{,\alpha} + \varphi_{,\alpha} \psi^\varepsilon_{,3}) + \\ & + \hat{\mu}_{\alpha i 33}(\varphi^\varepsilon_{,\alpha} v_{i,33} - \psi_{,\alpha} u^\varepsilon_{i,33}) + (\hat{\mu}_{3i\alpha 3} + \hat{\mu}_{3i3\alpha})(\varphi^\varepsilon_{,3} v_{i,3\alpha} - \psi_{,3} u^\varepsilon_{i,3\alpha}) \big\} \, dx, \\ a_2(s^\varepsilon, r) := & \int_B \big\{ \hat{c}_{i\alpha j\beta} u^\varepsilon_{j,\beta} v_{i,\alpha} + \hat{p}_{\alpha\beta i}(\varphi^\varepsilon_{,\alpha} v_{i,\beta} - \psi_{,\alpha} u^\varepsilon_{i,\beta}) + \hat{\kappa}_{\alpha\beta} \varphi^\varepsilon_{,\beta} \psi_{,\alpha} + \\ & + \hat{\mu}_{3i\alpha\beta}(\varphi^\varepsilon_{,3} v_{i,\alpha\beta} - \psi_{,3} u^\varepsilon_{i,\alpha\beta}) + (\hat{\mu}_{\beta\alpha i 3} + \hat{\mu}_{\beta i 3\alpha})(\varphi^\varepsilon_{,\beta} v_{i,3\alpha} - \psi_{,\beta} u^\varepsilon_{i,3\alpha}) \big\} \, dx, \\ a_3(s^\varepsilon, r) := & \int_B \hat{\mu}_{\sigma i\alpha\beta}(\varphi^\varepsilon_{,\sigma} v_{i,\alpha\beta} - \psi_{,\sigma} u^\varepsilon_{i,\alpha\beta}) dx. \end{aligned}$$

The polynomial structure of the rescaled problem (4) in terms of ε suggests to develop the solution s^ε as a series of powers of ε:

$$\begin{array}{l} s^\varepsilon = s^0 + \varepsilon s^1 + \varepsilon^2 s^2 + \ldots, \\ \bar{s}^\varepsilon = \bar{s}^0 + \varepsilon \bar{s}^1 + \varepsilon^2 \bar{s}^2 + \ldots, \\ \hat{s}^\varepsilon = \hat{s}^0 + \varepsilon \hat{s}^1 + \varepsilon^2 \hat{s}^2 + \ldots. \end{array} \tag{5}$$

where $\bar{s}^\varepsilon = s^\varepsilon \circ \bar{\pi}^\varepsilon$ and $\hat{s}^\varepsilon = s^\varepsilon \circ \hat{\pi}^\varepsilon$. By inserting (5) into the rescaled problem (4), and by identifying the terms with identical power of ε, as customary, a set of variational problems is obtained to be solved in order to characterize the limit flexoeletric state s^0 and its associated limit problem.

4. Flexoelectric imperfect contact conditions

In this section, the imperfect flexoeletric contact model corresponds to an adhesive which is weaker with respect to the adherents. The following set of variational problems $\mathcal{P}_q$ is obtained from the asymptotic analysis:

$$\left\{\begin{array}{ll} \mathcal{P}_0: & \bar{A}_-(s^0,r)+\bar{A}_+(s^0,r)+a_0(s^0,r)=L(r),\\ \mathcal{P}_1: & \bar{A}_-(s^1,r)+\bar{A}_+(s^1,r)+a_0(s^1,r)+a_1(s^0,r)=0,\\ \mathcal{P}_q: & \bar{A}_-(s^q,r)+\bar{A}_+(s^q,r)+a_0(s^q,r)+a_1(s^{q-1},r)+a_2(s^{q-2},r)=0,\ q\geq 2. \end{array}\right.$$

Let us focus on problem $\mathcal{P}_0$. The integration by parts is performed by means of the Gauss-Green theorem, as follows:

$$\begin{aligned} &-\int_{\Omega_\pm}\left\{\bar{\sigma}^0_{ij,j}v_i-\bar{D}^0_{i,i}\psi\right\}dx+\int_{\Gamma_1}\left\{\bar{T}^0_i v_i+\bar{R}^0_i\partial_n v_i-\bar{D}^0_i n_i\psi\right\}d\Gamma-\\ &-\int_B\left(\hat{\mathbf{c}}\mathbf{u}^0_{,33}+\hat{\mathbf{p}}\varphi^0_{,33}-\hat{\boldsymbol{\mu}}\varphi^0_{,333}\right)\cdot\mathbf{v}dx-\\ &-\int_B\left(\hat{\kappa}\varphi^0_{,33}-\hat{\mathbf{p}}\cdot\mathbf{u}^0_{,33}-\hat{\boldsymbol{\mu}}\cdot\mathbf{u}^0_{,333}\right)\psi dx\mp\\ &\mp\int_{S_\pm}\left(\bar{\boldsymbol{\Sigma}}^0-\hat{\mathbf{c}}\mathbf{u}^0_{,3}-\hat{\mathbf{p}}\varphi^0_{,3}+\hat{\boldsymbol{\mu}}\varphi^0_{,33}\right)|_{x_3=\pm\frac{1}{2}}\cdot\mathbf{v}d\Gamma\mp\\ &\mp\int_{S_\pm}\left(\bar{\tilde{\boldsymbol{\sigma}}}^0-\hat{\boldsymbol{\mu}}\varphi^0_{,3}\right)|_{x_3=\pm\frac{1}{2}}\cdot\mathbf{v}_{,3}d\Gamma\pm\\ &\pm\int_{S_\pm}\left(\bar{D}^0_3+\hat{\kappa}\varphi^0_{,3}-\hat{\mathbf{p}}\cdot\mathbf{u}^0_{,3}-\hat{\boldsymbol{\mu}}\cdot\mathbf{u}^0_{,33}\right)|_{x_3=\pm\frac{1}{2}}\psi d\Gamma=L(r), \end{aligned}\tag{6}$$

where $\mathbf{n}(\tilde{x},\pm\frac{1}{2})=\mp\mathbf{e}_3$ on $S_\pm$, $\hat{\mathbf{c}}:=(\hat{c}_{i3j3})$, $\hat{\mathbf{p}}:=(\hat{p}_{3i3})$, $\hat{\kappa}:=\hat{\kappa}_{33}$, and $\hat{\boldsymbol{\mu}}:=(\hat{\mu}_{i333})$. $\bar{\boldsymbol{\Sigma}}^0:=(\bar{\sigma}^0_{i3}+\bar{\tilde{\sigma}}^0_{i\alpha3,\alpha})$ and $\bar{\tilde{\boldsymbol{\sigma}}}^0:=(\bar{\tilde{\sigma}}^0_{i33})$ represent, respectively, the physical and the higher-order traction vectors evaluated at the interfaces $S_\pm$. From equation (6), using standard variational arguments, the following set of equilibrium equations is derived:

$$\left\{\begin{array}{ll} \bar{\sigma}^0_{ij,j}+f_i=0,\quad \bar{D}^0_{i,i}=\rho^e & \text{in } \Omega_\pm,\\ \bar{T}^0_i=g_i,\quad \bar{R}^0_i=r_i,\quad \bar{D}^0_i n_i=-w & \text{on } \Gamma_1,\\ \bar{u}^0_i=0,\quad \partial_n\bar{u}^0_i=0,\quad \bar{\varphi}^0=0 & \text{on } \Gamma_0,\\ \hat{\mathbf{c}}\hat{\mathbf{u}}^0_{,33}+\hat{\mathbf{p}}\hat{\varphi}^0_{,33}-\hat{\boldsymbol{\mu}}\hat{\varphi}^0_{,333}=\mathbf{0} & \text{in } B,\\ \hat{\kappa}\hat{\varphi}^0_{,33}-\hat{\mathbf{p}}\cdot\hat{\mathbf{u}}^0_{,33}-\hat{\boldsymbol{\mu}}\cdot\hat{\mathbf{u}}^0_{,333}=0 & \text{in } B,\\ \mp\left(\bar{\boldsymbol{\Sigma}}^0-\hat{\mathbf{c}}\hat{\mathbf{u}}^0_{,3}-\hat{\mathbf{p}}\hat{\varphi}^0_{,3}+\hat{\boldsymbol{\mu}}\hat{\varphi}^0_{,33}\right)|_{x_3=\pm\frac{1}{2}}=\mathbf{0} & \text{on } S_\pm,\\ \pm\left(\bar{D}^0_3+\hat{\kappa}\hat{\varphi}^0_{,3}-\hat{\mathbf{p}}\cdot\hat{\mathbf{u}}^0_{,3}-\hat{\boldsymbol{\mu}}\cdot\hat{\mathbf{u}}^0_{,33}\right)|_{x_3=\pm\frac{1}{2}}=0 & \text{on } S_\pm,\\ \mp\left(\bar{\tilde{\boldsymbol{\sigma}}}^0-\hat{\boldsymbol{\mu}}\hat{\varphi}^0_{,3}\right)|_{x_3=\pm\frac{1}{2}}=\mathbf{0} & \text{on } S_\pm. \end{array}\right.\tag{7}$$

Equations $(7)_{1,2,3}$ represent the equilibrium equations at order 0 on the adherents with the suitable boundary conditions. Equations $(7)_{4,5}$ allows to characterize the explicit expressions of the displacement field and electric potential within the interface layer B, and combined with $(7)_{6,7,8}$, the interface conditions can be easily derived. Let us integrate $(7)_{4,5}$ along x_3. One gets:

$$\begin{aligned} &\hat{\mathbf{c}}\hat{\mathbf{u}}^0_{,3} + \hat{\mathbf{p}}\hat{\varphi}^0_{,3} - \hat{\boldsymbol{\mu}}\hat{\varphi}^0_{,33} = \mathbf{c}_1, \\ &\hat{\kappa}\hat{\varphi}^0_{,3} - \hat{\mathbf{p}}\cdot\hat{\mathbf{u}}^0_{,3} - \hat{\boldsymbol{\mu}}\cdot\hat{\mathbf{u}}^0_{,33} = d_1, \end{aligned} \tag{8}$$

where $\mathbf{c}_1 = (c_{1i})$ and d_1 are independent of x_3. By virtue of the continuity conditions for the displacements, normal derivative of the displacements, and electric potential at the interface $S_\pm$, the constant term d_1 can be immediately determined, having the following known form: $d_1 = \hat{\kappa}[\varphi^0] - \hat{\mathbf{p}}\cdot[\mathbf{u}^0] - \hat{\boldsymbol{\mu}}\cdot[\mathbf{u}^0_{,3}]$. By manipulating the system of equations (8), one has:

$$\begin{aligned} &\tfrac{1}{\hat{\kappa}}(\hat{\boldsymbol{\mu}}\otimes\hat{\boldsymbol{\mu}})\hat{\mathbf{u}}^0_{,33} - \tfrac{1}{\hat{\kappa}}(\hat{\mathbf{p}}\otimes\hat{\boldsymbol{\mu}} - \hat{\boldsymbol{\mu}}\otimes\hat{\mathbf{p}})\hat{\mathbf{u}}^0_{,3} - \left(\hat{\mathbf{c}} + \tfrac{1}{\hat{\kappa}}\hat{\mathbf{p}}\otimes\hat{\mathbf{p}}\right)\hat{\mathbf{u}}^0 = \mathbf{c}_0 + x_3\left(\mathbf{p}\tfrac{d1}{\hat{\kappa}} - \mathbf{c}_1\right), \\ &\hat{\varphi}^0_{,3} = \tfrac{1}{\hat{\kappa}}(d_1 + \hat{\mathbf{p}}\cdot\hat{\mathbf{u}}^0_{,3} + \hat{\boldsymbol{\mu}}\cdot\hat{\mathbf{u}}^0_{,33}), \end{aligned} \tag{9}$$

where $\mathbf{c}_0 = (c_{0i})$ is independent of x_3. To explicitly characterize the expression of $\mathbf{u}^0$ and φ^0, a particular flexoelectric constitutive law is considered, namely a piezoelectric transversely isotropic material, with flexoelectric cubic symmetry (for more details, see Appendix A). In this special case, the adhesive constitutive matrices reduce to

$$\hat{\mathbf{c}} = \begin{pmatrix} \hat{c}_{44} & 0 & 0 \\ 0 & \hat{c}_{44} & 0 \\ 0 & 0 & \hat{c}_{33} \end{pmatrix}, \quad \hat{\mathbf{p}} = \begin{pmatrix} 0 \\ 0 \\ \hat{e}_{33} \end{pmatrix}, \quad \hat{\boldsymbol{\mu}} = \begin{pmatrix} 0 \\ 0 \\ \hat{\mu}_{11} \end{pmatrix}.$$

Taking into account the above material properties, equations (9) simplify into the following system:

$$\begin{aligned} &\hat{u}^0_\alpha = \tfrac{1}{\hat{c}_{44}}(c_{1\alpha}x_3 - c_{0\alpha}), \\ &\hat{u}^0_{3,33} - \gamma^2\hat{u}^0_3 = \tfrac{\hat{\kappa}}{\hat{\mu}^2_{11}}\left(c_{03} + x_3\left(\tfrac{\hat{e}_{33}}{\hat{\kappa}}d_1 - c_{13}\right)\right), \quad \text{with} \quad \gamma^2 := \tfrac{\hat{c}_{33}\hat{\kappa}+\hat{e}^2_{33}}{\hat{\mu}^2_{11}}, \\ &\hat{\varphi}^0_{,3} = \tfrac{1}{\hat{\kappa}}(d_1 + \hat{e}_{33}\hat{u}^0_{3,3} + \hat{\mu}_{11}\hat{u}^0_{3,33}). \end{aligned} \tag{10}$$

Thus, imposing the continuity conditions at the interface $S_\pm$, costants $\mathbf{c}_1$ and $\mathbf{c}_0$ can be determined and we obtain:

$$\begin{aligned} &\hat{u}^0_\alpha(\tilde{x}, x_3) = \langle u^0_\alpha, \rangle + x_3[u^0_\alpha], \quad \tilde{x} = (x_\alpha), \\ &\hat{u}^0_3(\tilde{x}, x_3) = A_0 + A_1x_3 + A_2e^{\gamma x_3} + A_3e^{-\gamma x_3}, \\ &\hat{\varphi}^0(\tilde{x}, x_3) = B_0 + B_1x_3 + B_2e^{\gamma x_3} + B_3e^{-\gamma x_3}, \end{aligned} \tag{11}$$

where A_i and B_i depend on the jump and mean values of the flexoelectric state $s^0 = (\mathbf{u}^0, \varphi^0)$ at the interfaces $S_\pm$:

$$
\begin{aligned}
&A_0 := \tfrac{\gamma\hat{\mu}_{11}^2}{2\hat{\kappa}(e^\gamma-1)}\left\{(1+e^\gamma)[u^0_{3,3}] - 2\gamma(e^\gamma-1)\langle u^0_3\rangle\right\},\\
&A_1 := \tfrac{1}{e^\gamma(\gamma-2)+\gamma+2}\left\{\gamma(1+e^\gamma)[u^0_3] - 2(e^\gamma-1)\langle u^0_{3,3}\rangle\right\},\\
&A_2 := \tfrac{e^{\gamma/2}}{\gamma(e^\gamma-1)(e^\gamma(\gamma-2)+\gamma+2)}\left\{(1-e^\gamma)[u^0_{3,3}] + \gamma(e^\gamma u^{0,+}_{3,3} - u^{0,-}_{3,3}) - \gamma(e^\gamma-1)[u^0_3]\right\},\\
&A_3 := \tfrac{e^{\gamma/2}}{\gamma(e^\gamma-1)(e^\gamma(\gamma-2)+\gamma+2)}\left\{(1-e^\gamma)[u^0_{3,3}] - \gamma(e^\gamma u^{0,-}_{3,3} - u^{0,+}_{3,3}) + \gamma(e^\gamma-1)[u^0_3]\right\},\\
&B_0 := \langle\varphi^0\rangle - \tfrac{\hat{e}_{33}}{\hat{\kappa}}(\langle u^0_3\rangle - A_0) - \tfrac{\hat{\mu}_{11}}{\hat{\kappa}}(\langle u^0_{3,3}\rangle - A_1),\\
&B_1 := [\varphi^0] - \tfrac{\hat{e}_{33}}{\hat{\kappa}}([u^0_3] - A_1) - \tfrac{\hat{\mu}_{11}}{\hat{\kappa}}[u^0_{3,3}],\\
&B_2 := \tfrac{\hat{e}_{33}+\gamma\hat{\mu}}{\hat{\kappa}}A_2, \quad B_3 := \tfrac{\hat{e}_{33}-\gamma\hat{\mu}}{\hat{\kappa}}A_3.
\end{aligned}
$$

with $f^\pm := f(\tilde{x}, \pm\frac{1}{2})$. As in classical elastic soft interface models [26, 28, 32], the in-plane displacements u^0_α are linear functions of the through-the-thickness coordinate x_3. While the transversal displacement u^0_3 and the electric potential φ^0 depend exponentially on x_3: this result is due to the particular second gradient flexoelectric continuum model employed in the derivation and will influence the expression of the imperfect contact conditions for soft flexoelectric interfaces.

By summing and subtracting equations $(7)_{6,7,8}$, combined with the expressions (11), one can evaluate the jumps $[\cdot]$ and mean values $\langle\cdot\rangle$ and establish the following set of transmission conditions for flexoelectric imperfect contact:

$$
\begin{cases}
[\Sigma^0_{i3}] = 0,\\
[D^0_3] = 0,\\
\langle\Sigma^0_{\alpha3}\rangle = \hat{c}_{44}[u^0_\alpha],\\
\langle\Sigma^0_{33}\rangle = \hat{c}_{33}[u^0_3] + \hat{e}_{33}[\varphi^0] - \frac{\hat{\mu}_{11}\hat{e}_{33}}{\hat{\kappa}_{33}}[u^0_{3,3}] + \hat{d}_{33}\lambda([u^0_3] - \langle u^0_{3,3}\rangle),\\
\langle D^0_3\rangle = -\hat{\kappa}_{33}[\varphi^0] + \hat{e}_{33}[u^0_3] + \hat{\mu}_{11}[u^0_{3,3}],\\
[\tilde{\sigma}^0_{\alpha33}] = 0,\\
\langle\tilde{\sigma}^0_{\alpha33}\rangle = 0,\\
[\tilde{\sigma}^0_{333}] = \frac{\hat{\mu}_{11}\hat{e}_{33}}{\hat{\kappa}_{33}}[u^0_{3,3}] - \hat{d}_{33}\lambda([u^0_3] - \langle u^0_{3,3}\rangle),\\
\langle\tilde{\sigma}^0_{333}\rangle = -\frac{\hat{\mu}_{11}\hat{e}_{33}}{\hat{\kappa}_{33}}([u^0_3] - \langle u^0_{3,3}\rangle) + \hat{\mu}_{11}[\varphi^0] + \frac{\hat{\mu}_{11}^2}{\lambda\hat{\kappa}_{33}}[u^0_{3,3}],
\end{cases}
\tag{12}
$$

with $\hat{d}_{33} := \hat{c}_{33} + \frac{\hat{e}^2_{33}}{\hat{\kappa}_{33}}$, and $\lambda := \frac{2(e^\gamma-1)}{e^\gamma(\gamma-2)+\gamma+2}$, and $[f] := f(\tilde{x}, 1/2) - f(\tilde{x}, -1/2)$ and $\langle f\rangle := \frac{1}{2}(f(\tilde{x}, 1/2) + f(\tilde{x}, -1/2))$. We can note that $\hat{\mu}_{11}[\varphi^0_{,3}] = \frac{\hat{\mu}_{11}\hat{e}_{33}}{\hat{\kappa}_{33}}[u^0_{3,3}] - \hat{d}_{33}\lambda([u^0_3] - \langle u^0_{3,3}\rangle)$ and, thus, $\langle\Sigma^0_{33}\rangle = \hat{c}_{33}[u^0_3] + \hat{e}_{33}[\varphi^0] - \hat{\mu}_{11}[\varphi^0_{,3}]$ and $[\tilde{\sigma}^0_{333}] = \hat{\mu}_{11}[\varphi^0_{,3}]$.

Remark 1. The transmission problems for a soft flexoelectric interface at order 0 represent a formal generalization of the soft interface models obtained by means of the asymptotic methods in linear elasticity [32] and in other multifield frameworks [33, 34], such as piezoelectricity [38], magneto-electro-thermo-elasticity [39, 37] and microstructural theories [39, 36]. The soft interface model presents a similar structure at order 0 as, for instance, in linear elastic asymptotic models. At order 0, the interface shows a discontinuity of the flexoelectric state s_0, namely displacements, normal derivatives of the displacements and electric potential. The interphase layer behaves from a mechanical point of view as a series of springs, reacting to the gap between the top and bottom flexoelectric state. The physical traction vector (Σ^0_{i3}) and normal electric displacement D^0_3 at the interface remain continuous. The higher-order traction $\tilde{\sigma}^0_{333}$ presents a discontinuity, which is not expected and predicted as in classical linear elastic or piezoelectric continuum theories and is likely due to the second gradient nature of the chosen direct flexoelectric model. Surface elastic or piezoelectric effects do not appear in asymptotic models for soft (spring-type) interfaces, at order 0. In order to highlight surface effects, it is necessary to characterize the higher-order model, at order 1, see [33].

Remark 2. The flexoelectric contact law (4) at order 0 reduces to the soft interface piezoelectric interface conditions by letting the flexoelectric coefficient $\hat{\mu}_{11}$ vanish. Indeed,

$$\lim_{\mu_{11}\to 0} \lambda(\mu_{11}) = \lim_{\gamma\to\infty} \lambda(\gamma) = 0 \quad \text{and} \quad \lim_{\mu_{11}\to 0} \frac{\mu_{11}^2}{\lambda(\mu_{11})} = 0.$$

Consequently, by neglecting the contribution of the flexoelectric effect, the hyper-stresses can also be discarded, giving $\tilde{\sigma}^0_{i33} = 0$, and $\Sigma^0_{i3} = \check{\sigma}^0_{i3}$, i.e., the physical stress coincides with the Cauchy stress. Thus, the transmission conditions become

$$\begin{cases} [\check{\sigma}^0_{i3}] = 0, \\ [D^0_3] = 0, \\ \langle \check{\sigma}^0_{\alpha 3} \rangle = \hat{c}_{44}[u^0_\alpha], \\ \langle \check{\sigma}^0_{33} \rangle = \hat{c}_{33}[u^0_3] + \hat{e}_{33}[\varphi^0], \\ \langle D^0_3 \rangle = -\hat{\kappa}_{33}[\varphi^0] + \hat{e}_{33}[u^0_3]. \end{cases}$$

As found in [34, 38], the above conditions are typical of lowly-conducting and mechanically compliant transversely isotropic piezoelectric adhesives, also known as soft piezoelectric adhesives.

Finally, by applying the inverse coordinate change $(\pi^\varepsilon)^{-1}$, and knowing that $\hat{\mathbf{c}} = \frac{1}{\varepsilon}\hat{\mathbf{c}}^\varepsilon$, $\hat{\mathbf{p}} = \frac{1}{\varepsilon}\hat{\mathbf{p}}^\varepsilon$, $\hat{\kappa} = \frac{1}{\varepsilon}\hat{\kappa}^\varepsilon$, and $\hat{\boldsymbol{\mu}} = \frac{1}{\varepsilon^2}\hat{\boldsymbol{\mu}}^\varepsilon$, the interface conditions (4) can be scaled back onto the original domain Ω^ε (see Fig. 1), as follows:

$$\begin{cases} [\Sigma^\varepsilon_{i3}] = 0, \\ [D^\varepsilon_3] = 0, \\ \langle \Sigma^\varepsilon_{\alpha 3} \rangle = \frac{1}{\varepsilon}\hat{c}^\varepsilon_{44}[u^\varepsilon_\alpha], \\ \langle \Sigma^\varepsilon_{33} \rangle = \frac{1}{\varepsilon}\left(\hat{c}^\varepsilon_{33}[u^\varepsilon_3] + \hat{e}^\varepsilon_{33}[\varphi^\varepsilon] - \frac{\hat{\mu}^\varepsilon_{11}\hat{e}^\varepsilon_{33}}{\hat{\kappa}^\varepsilon_{33}}[u^\varepsilon_{3,3}] + \hat{d}^\varepsilon_{33}\lambda^\varepsilon([u^\varepsilon_3] - \varepsilon\langle u^\varepsilon_{3,3}\rangle)\right), \\ \langle D^\varepsilon_3 \rangle = \frac{1}{\varepsilon}\left(-\hat{\kappa}^\varepsilon_{33}[\varphi^\varepsilon] + \hat{e}^\varepsilon_{33}[u^\varepsilon_3] + \hat{\mu}^\varepsilon_{11}[u^\varepsilon_{3,3}]\right), \\ [\tilde{\sigma}^\varepsilon_{\alpha 33}] = 0, \\ \langle \tilde{\sigma}^\varepsilon_{\alpha 33} \rangle = 0, \\ [\tilde{\sigma}^\varepsilon_{333}] = \frac{1}{\varepsilon}\left(\frac{\hat{\mu}^\varepsilon_{11}\hat{e}^\varepsilon_{33}}{\hat{\kappa}^\varepsilon_{33}}[u^\varepsilon_{3,3}] - \hat{d}^\varepsilon_{33}\lambda^\varepsilon([u^\varepsilon_3] - \varepsilon\langle u^\varepsilon_{3,3}\rangle)\right), \\ \langle \tilde{\sigma}^\varepsilon_{333} \rangle = \frac{1}{\varepsilon^2}\left(-\frac{\hat{\mu}^\varepsilon_{11}\hat{e}^\varepsilon_{33}}{\hat{\kappa}^\varepsilon_{33}}([u^\varepsilon_3] - \varepsilon\langle u^\varepsilon_{3,3}\rangle) + \hat{\mu}^\varepsilon_{11}[\varphi^\varepsilon] + \frac{(\hat{\mu}^\varepsilon_{11})^2}{\lambda^\varepsilon\hat{\kappa}^\varepsilon_{33}}[u^\varepsilon_{3,3}]\right), \end{cases} \tag{13}$$

where $\hat{d}^\varepsilon_{33} = \varepsilon\hat{d}_{33}$, $\gamma^\varepsilon = \varepsilon\gamma$, $\lambda^\varepsilon := \frac{2(e^{\frac{\gamma^\varepsilon}{\varepsilon}}-1)}{e^{\frac{\gamma^\varepsilon}{\varepsilon}}(\frac{\gamma^\varepsilon}{\varepsilon}-2)+\frac{\gamma^\varepsilon}{\varepsilon}+2}$. The obtained transmission conditions can be implemented in the simple numerical example presented in the following section.

5. A closed-form solution for one-dimensional flexoelectric imperfect contact problems

In this section, the closed-form solution for the one-dimensional equilibrium problem of a flexoelectric three-layer micro-bar is presented. Moreover, the exact solution of the three-layer one-dimensional problem will be compared with the solution of a two-phase composite micro-bar, in which the intermediate layer is replaced by the imperfect contact conditions (13) (see Section 4).

In the sequel, for the sake of brevity, we omitted the dependences on ε of the unknown functions and constitutive coefficients. The geometry of the one-dimensional composite micro-beam is illustrated in Fig. 2. The bar axis is identified with the abscissa x, the adherents are $\Omega_- := (0, L)$, $\Omega_+ := (L+\varepsilon, 2L+\varepsilon)$, and the adhesive $B := (L, L+\varepsilon)$, with $\varepsilon << L$. The boundary $\Gamma_0 = \{0\}$ is fully clamped, while $\Gamma_1 = \{2L+\varepsilon\}$ is a free end.

The one-dimensional flexoelectric equilibrium equations take the following form on each domain Ω_-, Ω_+ and B, respectively:

$$\begin{cases} cu'' + p\varphi'' - \mu\varphi''' = 0, \\ pu'' + \mu u''' - k\varphi'' = 0, \end{cases}$$

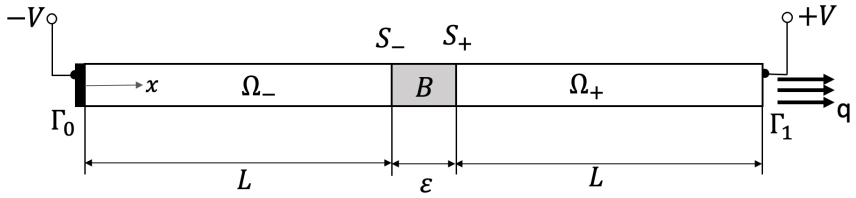

Figure 2: One-dimensional flexoelectric composite bar under tensile load

where $(\cdot)' := \frac{d}{dx}(\cdot)$, c, p, μ, k represent the elastic, piezoelectric, flexoelectric and dielectric material moduli, respectively. The system can be decoupled, as customary,

$$\begin{cases} \varphi'' = \frac{1}{k}(pu'' + \mu u''') \\ u'''' - \gamma^2 u'' = 0, \ \gamma^2 := \frac{ck+p^2}{\mu^2}, \end{cases} \tag{14}$$

and the closed-form solution, defined on each sub-domain, takes the following form:

$$u(x) = c_0 + c_1 x + c_3 e^{\gamma x} + c_4 e^{-\gamma x}, \ \ \varphi(x) = c_5 + c_6 x + c_3 \frac{e+\mu\gamma}{k} e^{\gamma x} + c_4 \frac{e-\mu\gamma}{k} e^{-\gamma x},$$

with c_i are constants to be determined by applying the boundary conditions on Γ_0 and Γ_1, and interface conditions on $S_\pm$. Two types of electromechanical loading conditions will be tested: BC_1 is associated with an applied electric potential difference $\pm V$ acting on Γ_0 and Γ_1, without any mechanical charges; BC_2 corresponds to the case of a prescribed tensile traction q on Γ_1, with no electric loads. The conditions on the extremities take the following form:

$$BC_1 : \begin{cases} u(0) = 0, & u'(0) = 0, & \varphi(0) = -V, & \text{on } \Gamma_0, \\ \sigma(2L+\varepsilon) = 0 & \tilde{\sigma}(2L+\varepsilon) = 0, & \varphi(2L+\varepsilon) = V, & \text{on } \Gamma_1. \end{cases}$$

$$BC_2 : \begin{cases} u(0) = 0, & u'(0) = 0, & \varphi(0) = 0, & \text{on } \Gamma_0, \\ \sigma(2L+\varepsilon) = q & \tilde{\sigma}(2L+\varepsilon) = 0, & D(2L+\varepsilon) = 0, & \text{on } \Gamma_1. \end{cases}$$

Note that the boundary conditions for both the exact three-phase model and two-phase model with imperfect contact are identical. For the three-layers composite bar, classical interface continuity conditions (CC) are considered on $S_\pm$, namely $x = L$ and $x = L + \varepsilon$, so that

$$CC : \begin{cases} [u] = 0, & [u'] = 0, & [\varphi] = 0, \\ [\sigma] = 0, & [\tilde{\sigma}] = 0, & [D] = 0. \end{cases}$$

Concerning the two-layers composite bar with imperfect contact (IC), the

soft interface conditions (13) on $S_\pm$ are adapted for the one-dimensional case:

$$IC: \begin{cases} [\sigma] = 0, \\ \langle\sigma\rangle = \frac{1}{\varepsilon}\left(c[u] + p[\varphi] - \frac{\mu p}{k}[u'] + d\lambda([u] - \varepsilon\langle u'\rangle)\right), \\ [D] = 0, \\ \langle D\rangle = \frac{1}{\varepsilon}\left(-k[\varphi] + p[u] + \mu[u']\right), \\ [\tilde{\sigma}] = \frac{1}{\varepsilon}\left(\frac{\mu p}{k}[u'] - d\lambda([u] - \varepsilon\langle u'\rangle)\right), \\ \langle\tilde{\sigma}\rangle = \frac{1}{\varepsilon^2}\left(\mu[\varphi] - \frac{\mu p}{k}([u] - \varepsilon\langle u'\rangle) + \frac{\mu^2}{k\lambda}[u']\right), \end{cases}$$

with $d := c + p^2/k$.

The adherents $\Omega_\pm$ are constituted by $SrTiO_3$ (Strontium Titanate), while the adhesive B is made of $BaTiO_3$ (Barium Titanate), whose material properties are shown in Table 1.

Moduli	$SrTiO_3$ ($\Omega_\pm$)	$BaTiO_3$ (B)
c, GPa	350	151
p, C/m^2	8.82	17.5
k, F/m	$3.45{\cdot}10^{-8}$	$1.16{\cdot}10^{-8}$
μ, C/m	$1{\cdot}10^{-4}$	$5{\cdot}10^{-4}$

Table 1: Constitutive material properties for $SrTiO_3$ and $BaTiO_3$, [8, 51]

Remark 3. The proposed formulation of flexoelectricity is able to capture possible non-local effects. Even though strain gradient elasticity, generally associated with one or more mechanical length-scale parameters, has been neglected in the expression of the electric Gibbs energy $\mathcal{G}$, the present modeling of flexoelectricity shows a particular size-dependency, related to a flexoelectric characteristic length. This phenomenon can be highlighted by means of the simple one-dimensional closed-form solution of the flexoelectric equilibrium problem (14). Equation $(14)_2$ can be rewritten as follows:

$$u'' - g^2 u'''' = 0,$$

where $g := \frac{1}{\gamma} = \frac{\mu}{\sqrt{ck+p^2}}$ is interpreted as a flexoelectric material length, directly related to the flexoelectric coefficient μ. The above equation is equivalent to the static equilibrium problem of strain gradient bars in tension, see, e.g. [52]. Fig. 3 and Fig. 4 show the variations of the displacement u, the deformation $\epsilon := u'$ and electric potential φ versus the dimensionless length x/L, varying the values of g, for a flexoelectric bar subject to a tensile load (dashed lines). The curves are compared with the classical solution of a

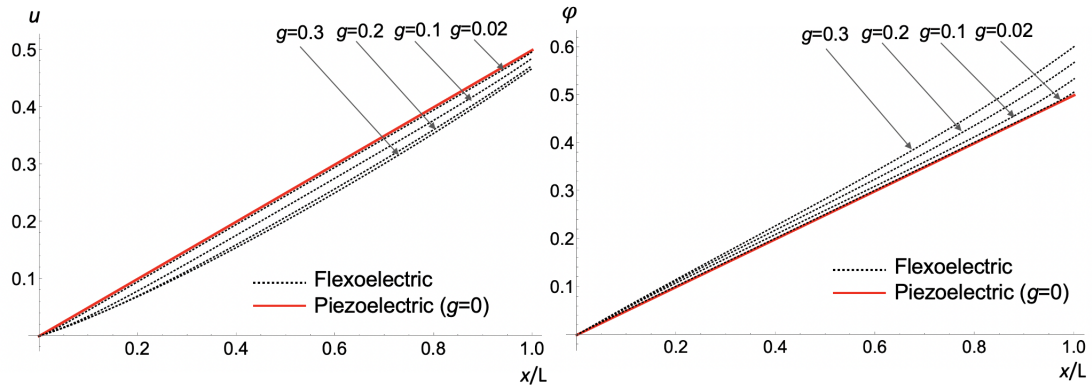

Figure 3: Displacement and electric potential vs x/L, for various values of g

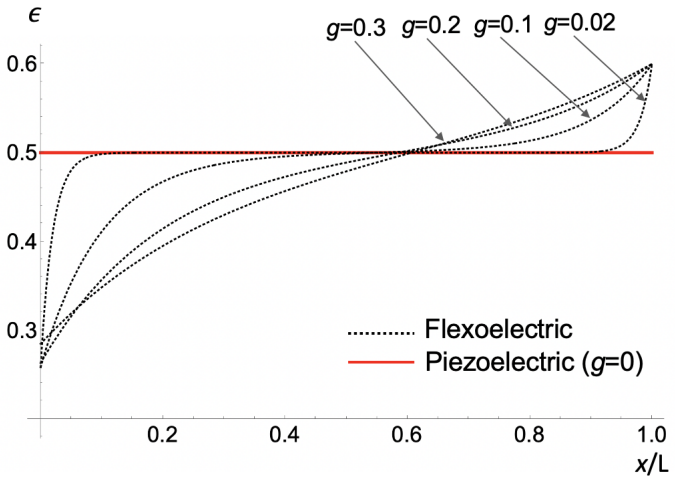

Figure 4: Deformation vs x/L, for various values of g

piezoelectric bar (red line), where the flexoelectric contribution is discarded, i.e., $g = 0$.

The plots reveal interesting conclusions. It is observed that the flexoelectric solution for the displacement field decreases for increasing values of g, showing a stiffness-softening. The piezoelectric solution, $g = 0$, is an upper-bound. The electric potential tends to increase with increasing values of g, hence the piezoelectric solution represents a lower-bound. Concerning the deformations, the present flexoelectric theory is capable of predicting end-effect ($g < 0.1$) or strain localization phenomena.

5.1. The applied electric potential difference

In this section, we study the case of two electric potentials $V = \pm 25\text{V}$, applied on both the two extremities of the composite micro-beam, of half-length $L = 10\ \mu\text{m}$, corresponding to BC_1 (see Fig. 2). No mechanical loading is considered in this example.

Following the ideas proposed in [34], the numerical results for the variables are provided using the dimensionless units. For an applied electric potential V, we set:

$$(U, \Phi) = \frac{E_0}{V}\left(u, \frac{\varphi}{E_0}\right), \qquad (\Sigma, \Delta, \tilde{\Sigma}) = \frac{LE_0}{C_{00}V}\left(\sigma, E_0 D, \frac{\tilde{\sigma}}{L}\right)$$

where, for numerical convenience, $E_0 = 10^9\ \text{Vm}^{-1}$ and $C_{00} = 1$ GPa.

First, the influence of the relative thickness of the adhesive $\frac{\varepsilon}{L}$ is investigated in order to evaluate the accuracy of the asymptotic modeling. In particular, the quality of the solutions is evaluated considering the L^2-relative errors $\frac{\|U-U_{model}\|}{\|U\|}$ and $\frac{\|\Phi-\Phi_{model}\|}{\|\Phi\|}$, where U and Φ indicate the exact solutions computed using the three-phase problem, while U_{model} and Φ_{model} denote the solutions of the two-phase model with imperfect contact (13). The convergence of the interface model towards the three-phase one with respect to the thickness ratio $\frac{\varepsilon}{L}(\%)$ is presented in Fig. 5. From Fig. 5, it can be observed

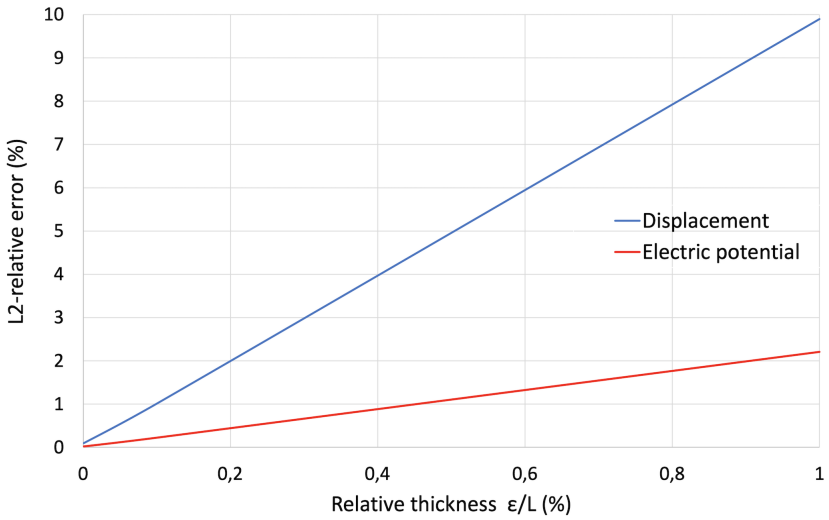

Figure 5: Convergence results with respect to the relative thickness ε/L

that, by reducing the thickness of the adhesive, the L^2-relative error presents a significant reduction, linearly decreasing with respect to ε/L. Hence, the proposed asymptotic imperfect contact model well-approximates the exact

solution, especially for small thickness ratios, and provides an acceptable solution. Indeed, passing from a relative thickness of 1% to 0.1%, the error drastically drops from 9.89% to 1.01%, concerning the displacement field, and from 2.21% to 0.22%, for the electric potential. Clearly, due to the plot linear trend, the reduction of an order of magnitude of ε/L implies the consequent decrease of an order of magnitude of the relative error.

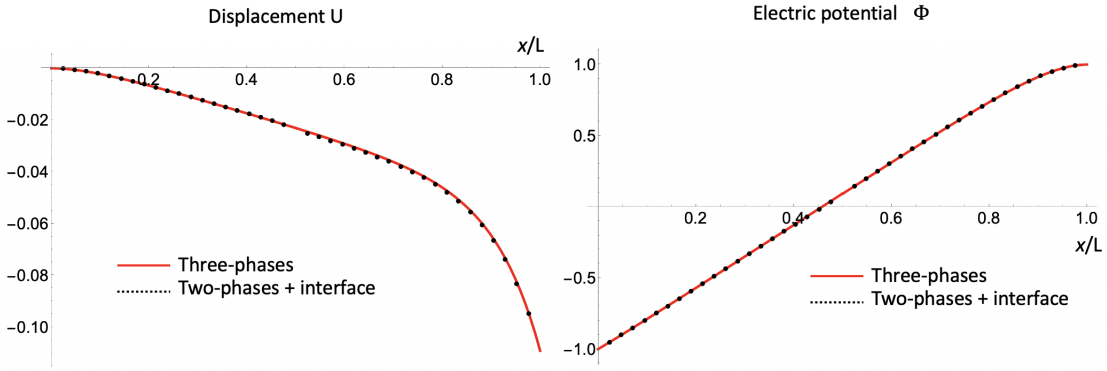

Figure 6: Dimensionless displacement and electric potential vs x/L, for $\varepsilon/L = 0.1\%$

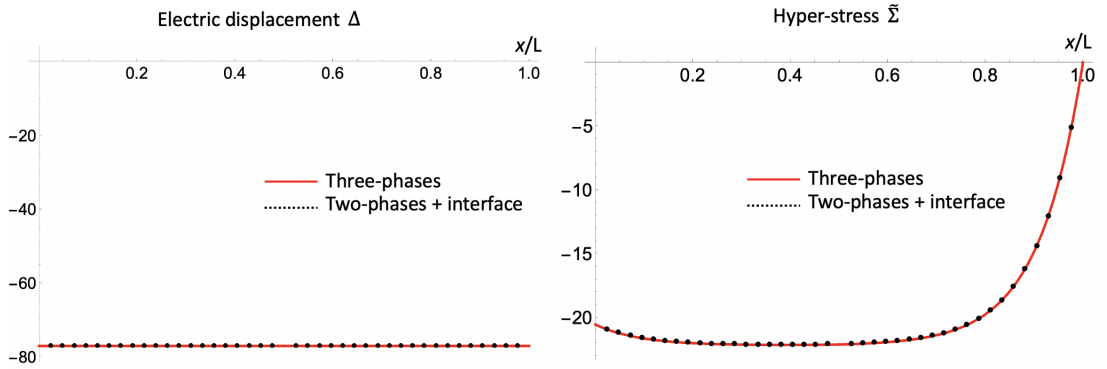

Figure 7: Dimensionless electric displacement and hyper-stress vs x/L, for $\varepsilon/L = 0.1\%$

Fig. 6 and Fig. 7 depict a comparison between the solutions of the three-phase problem and two-phase with imperfect interface, obtained through the asymptotic approximation. In this case, the relative thickness of the interface is fixed to 0.1%. Fig. 6 and Fig. 7 represent the trend of the dimensionless displacement field, electric potential, electric displacement and hyper-stress along the composite bar relative length. The stress field has not been plotted

since in both cases is equal to zero. The plots show a very good agreement between the solution of the three-layers problem (red solid line) and the solution of the reduced model (blue dashed line). Due to the second gradient nature of the problem, the displacement and electric potential exponentially vary along the beam length. The general trend is well-approximated by the asymptotic model. Negligible deviations can be found at the interface level since the material of the adhesive layer cannot be considered mechanically compliant and lowly conducting, asymptotically speaking. Indeed, the ratio among the adherents and adhesive constitutive coefficients does not qualify the intermediate layer as "properly soft". In order to overcome this problem, the asymptotic model at order 0 could be enhanced by characterizing also the first order order corrector term of the expansion, giving a more precise approximation.

5.2. The applied tensile load

In this section, the case of a tensile load q=1 Pa, applied to the free end, is investigated, corresponding to BC_2 (see Fig. 2). No electric loadings are taken into account.

As previously shown, the numerical results are provided using the dimensionless units. For an applied pressure q, we set:

$$(U, \Phi) = \frac{C_{00}}{Lq}\left(u, \frac{\varphi}{E_0}\right), \qquad (\Sigma, \Delta, \tilde{\Sigma}) = \frac{1}{q}\left(\sigma, E_0 D, \frac{\tilde{\sigma}}{L}\right)$$

where $E_0 = 10^{12}$ Vm^{-1} and $C_{00} = 1000$ GPa.

As before, from Fig. 8, one can observe, as before, by decreasing the relative thickness ratio the L^2-relative error significantly diminishes. Considering ε/L= 0.1%, the errors is 0.11%, for the displacement, and 0.41% for the electric potential, respectively.

Fig. 9 and Fig. 10 illustrate a comparison between the exact three-layer solution and two-phase with imperfect interface one, in terms of dimensionless displacement, electric potential, stress and hyper-stress, for a fixed ε/L. The electric displacement plot has not been reported since it vanishes in both cases. The plots show that the asymptotic model well-approximates the behaviour of the three-layers composite beam. This is in agreement with the previous convergence diagram. A slight deviation can be perceived in correspondence of the interface due to the particular choice of involved real material properties.

6. Conclusions

A novel form of the imperfect interface law for flexoelectric composite has been proposed, based on an asymptotic approach. The order 0 interface

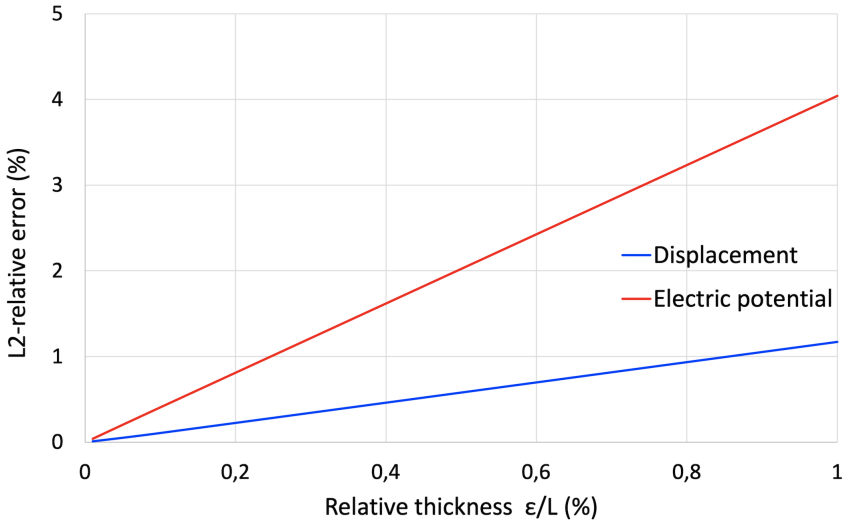

Figure 8: Convergence results with respect to the relative thickness ε/L

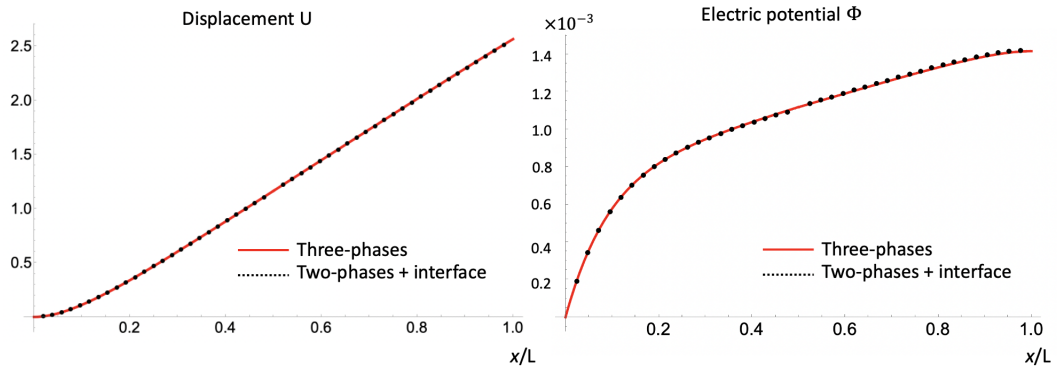

Figure 9: Dimensionless displacement and electric potential vs x/L, for $\varepsilon/L = 0.1\%$

conditions (4) corresponded to the case of soft flexoelectric adhesive and were given in terms of the mean values and jumps of the physical stress vector, normal electric displacement and higher-order traction, evaluated at the interface. The transmission conditions presented a similar structure compared to other soft adhesives in other different multiphysic frameworks [33], providing a discontinuity of the flexoelectric state in terms of u_i^0, $u_{i,3}^0$ and φ^0, and a continuity of the corresponding conjugated quantities (Σ_{i3}^0) and D_3^0. The interface model also highlighted an unexpected discontinuity of the hyperstress vector σ_{333}^0 at the interface, which could not be predicted in classical mechanical models.

Despite other proposed contact models for composite structures, e.g.

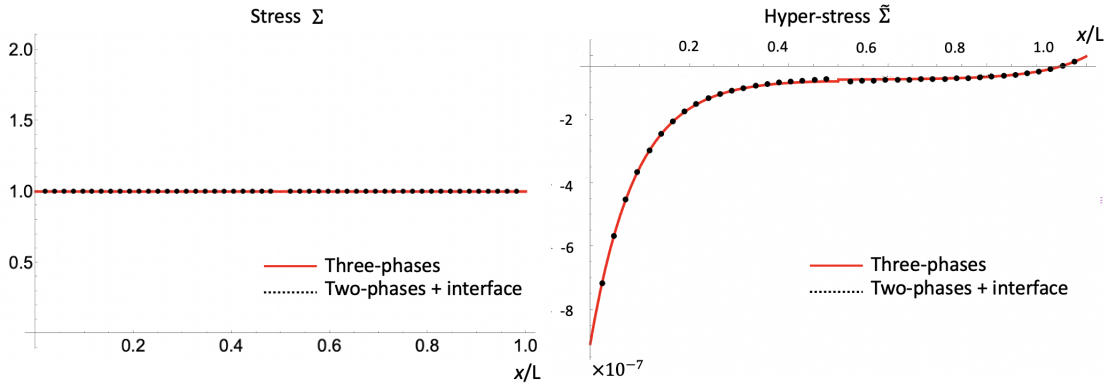

Figure 10: Dimensionless stress and hyper-stress vs x/L, for $\varepsilon/L = 0.1\%$

[53, 54], these conditions took into account the flexoelectric effect of the interface. Moreover, the formal asymptotic derivation allowed to consider the intrinsic second gradient nature of direct flexoelectricity, giving an unprecedented original form to the interface conditions.

In order to assess the validity of the previous asymptotic procedures, the analytical solution of a one-dimensional flexoelectric composite three-layers bar, alternatively subjected to a tensile load and an electric potential difference, has been developed. The numerical example took also into account the aforementioned imperfect contact laws. The convergence results showed that, by reducing the thickness of the adhesive, the relative error has a drastic reduction. Moreover, the numerical results reported a very good agreement between the exact three-layer solution and the two-layers solution with interface conditions in terms of electric potential, displacement, physical and higher-order stresses, and electric displacement, especially for thin adhesives.

The numerical example represents a preliminary numerical/analytical assessment of the obtained imperfect interface model. For an in-depth computational validation, the interface model needs to be implemented into a FE general code, providing full 3D numerical examples.

The proposed methodology proved to be efficient and simple-to use, and can be used in several applications, involving thin films and interfaces at micro-and nano-scales, such as in MEMS/NEMS, composite graphene structures, epitaxially strained films, contact problem in biological membranes, and more.

As future perspective, the first-order correction term of the asymptotic expansion will be characterized, allowing the definition of higher-order interface conditions as in [33]. Besides, the case of similar rigidities (hard

interface) will be investigated in order to characterize a generalized interface law for flexoelectric composites.

Acknowledgements

This research has been conducted under the auspices of the Italian National Group for the Mathematical Physics (GNFM) of the National Institute for Advanced Mathematics (INdAM). The financial support of the University of Ferrara via FAR grants 2020 and 2021 is gratefully acknowledged. R. Rodríguez-Ramos thanks the Department of Mathematics and Mechanics, IIMAS-UNAM for its support and the funding of PREI-DGAPA-UNAM. R. Rodríguez-Ramos acknowledges the funding of PAPIIT-DGAPA-UNAM IN101822, 2022-2023.

Appendix A.

Using Voigt's notation, the constitutive matrices of a transversely isotropic piezoelectric material are defined as follows (see [8, 10, 46]):

$$(c_{ijhk}) = \begin{pmatrix} c_{11} & c_{12} & c_{13} & 0 & 0 & 0 \\ c_{12} & c_{11} & c_{13} & 0 & 0 & 0 \\ c_{13} & c_{13} & c_{33} & 0 & 0 & 0 \\ 0 & 0 & 0 & c_{44} & 0 & 0 \\ 0 & 0 & 0 & 0 & c_{44} & 0 \\ 0 & 0 & 0 & 0 & 0 & c_{66} \end{pmatrix}, \quad (p_{ijh}) = \begin{pmatrix} 0 & 0 & e_{31} \\ 0 & 0 & e_{31} \\ 0 & 0 & e_{33} \\ 0 & e_{15} & 0 \\ e_{15} & 0 & 0 \\ 0 & 0 & 0 \end{pmatrix}$$

$$(\kappa_{ij}) = \begin{pmatrix} \kappa_{11} & 0 & 0 \\ 0 & \kappa_{11} & 0 \\ 0 & 0 & \kappa_{33} \end{pmatrix}.$$

with $c_{66} := \frac{1}{2}(c_{11} - c_{12})$. Furthermore, by assuming a cubic symmetry, $c_{33} = c_{11}$, $c_{12} = c_{13}$, $c_{66} = c_{44}$, $\kappa_{11} = \kappa_{33}$, and the independent flexoelectric components reduce to three, namely, the longitudinal μ_{11}, the transversal μ_{12}, and the shear μ_{44} coefficients. In isotropic flexoeletricity, the above coefficients satisfy $\mu_{11} - \mu_{12} + 2\mu_{44} = 0$. The direct flexoelectric tensor (3×18-matrix) is given as

$$(\mu_{ijkl}) = \begin{pmatrix} \mu_{11} & \mu_{12} & \mu_{12} & 0 & 0 & 0 & 0 & 0 & 0 & 0 & 0 & \mu_{44} & 0 & 0 & 0 & 0 & \mu_{44} & 0 \\ 0 & 0 & 0 & 0 & 0 & \mu_{44} & \mu_{12} & \mu_{11} & \mu_{12} & 0 & 0 & 0 & 0 & 0 & 0 & \mu_{44} & 0 & 0 \\ 0 & 0 & 0 & 0 & \mu_{44} & 0 & 0 & 0 & 0 & \mu_{44} & 0 & 0 & \mu_{12} & \mu_{12} & \mu_{11} & 0 & 0 & 0 \end{pmatrix}.$$

Note that because of the difference in number of components of strain gradient $e_{ij,k}$ and electric field gradient $E_{i,j}$, the converse flexoelectric tensor (6×9-matrix) takes the following matrix form

$$(\mu_{ijkl}) = \begin{pmatrix} \mu_{11} & 0 & 0 & 0 & \mu_{12} & 0 & 0 & 0 & \mu_{12} \\ \mu_{12} & 0 & 0 & 0 & \mu_{11} & 0 & 0 & 0 & \mu_{12} \\ \mu_{12} & 0 & 0 & 0 & \mu_{12} & 0 & 0 & 0 & \mu_{11} \\ 0 & 0 & 0 & 0 & 0 & \mu_{44} & 0 & \mu_{44} & 0 \\ 0 & 0 & \mu_{44} & 0 & 0 & 0 & \mu_{44} & 0 & 0 \\ 0 & \mu_{44} & 0 & \mu_{44} & 0 & 0 & 0 & 0 & 0 \end{pmatrix}.$$

All the symmetries of the flexoelectric tensor can be found in [55].

References

[1] Bahl S., Nagar H., Singh I. Sehgal S., Smart materials types, properties and applications: A review, *Materials Today: Proceedings* **2020** *28*, 1302–1306.

[2] Kulkarni H., Zohaib K., Khusru A., Shravan Aiyappa K., Application of piezoelectric technology in automotive systems, *Mater. Today Proc.* **2018** *5*, 21299–21304.

[3] Wang S., Rong W., Wang L., Xie H., Sun L., Mills J.K., A survey of piezoelectric actuators with long working stroke in recent years: classifications, principles, connections and distinctions, *Mech. Syst. Signal Process* **2019** *123*, 591–605

[4] Ebrahimi F., Dabbagh A. Wave propagation analysis of embedded nanoplates based on a nonlocal strain gradient-based surface piezoelectricity theory, *The European Physical Journal Plus* **2017** *132*(11), 1–14.

[5] Narita F., Fox M., A review on piezoelectric, magnetostrictive, and magnetoelectric materials and device technologies for energy harvesting applications, *Adv. Eng. Mater.* **2018** *20*, 1–22.

[6] Ebrahimi F., Dabbagh A. Thermo-magnetic field effects on the wave propagation behavior of smart magnetostrictive sandwich nanoplates. *The European Physical Journal Plus* **2018** *133*(3), 1–12.

[7] Ebrahimi F., Dabbagh A., Rabczuk T. On wave dispersion characteristics of magnetostrictive sandwich nanoplates in thermal environments, *European Journal of Mechanics-A/Solids* **2021** *85*, 104130.

[8] Shu L., Liang R., Rao Z., Fei L., Ke S., Wang Y. Flexoelectric materials and their related applications: A focused review, *J. Adv. Ceram.* **2019**, *8*(2), 153–173.

[9] Wang B., Gu Y., Zhang S., Chen L.-Q. Flexoelectricity in solids: Progress, challenges, and perspectives, *Progress Mat. Sci.* **2019**, *106*, 100570.

[10] Le Quang H., He Q.C. , The number and types of all possible rotational symmetries for flexoelectric tensors, *Proc. R. Soc. A* **2011**, *467* (2132), 2369–2386.

[11] Baskaran S., Ramachandran N., He X., Thiruvannamalai S., Lee H.J., Heo H., Chen Q., Fu J. Y., Giant flexoelectricity in polyvinylidene fluoride films, *Phys. Lett. A* **2011**, *375*, 2082.

[12] Baskaran S., He X.,Wang Y., Fu J.Y., Strain gradient induced electric polarization in α-phase polyvinylidene fluoride films under bending conditions, *J. Appl. Phys.* **2012**, *111*, 014109.

[13] Vasquez-Sancho F., Abdollahi A. , Damjanovic D., Catalan G., Flexoelectricity in bones *Adv. Mater.* **2018**, *30* (9), 1705316.

[14] Merupo V.I., Guiffard B. , Seveno R., Tabellout M., Kassiba A., Flexoelectric response in soft polyurethane films and their use for large curvature sensing, *J. Appl. Phys.* **2017**, *122*, 144101.

[15] Guiffard B., Saadeh M., Frère P., Seveno R., El-Gibari M., Sghaier T., Merupo V., and Kassiba A., Potentialities of flexoelectric effect in soft polymer films for electromechanical applications, *J. Phys.: Conf. Ser.* **2019**, *1322*, 012041.

[16] Ebrahimi F., Barati M.R. Surface effects on the vibration behavior of flexoelectric nanobeams based on nonlocal elasticity theory, *The European Physical Journal Plus* **2017** *132*(1), 1–13.

[17] Ebrahimi F., Karimiasl M. Nonlocal and surface effects on the buckling behavior of flexoelectric sandwich nanobeams, *Mechanics of Advanced Materials and Structures* **2018** *25*(11), 943–952.

[18] Ebrahimi F., Karimiasl M., Civalek Ö., Vinyas M. Surface effects on scale-dependent vibration behavior of flexoelectric sandwich nanobeams, *Advances in nano research* **2018** *7*(2), 77.

[19] Ebrahimi F., Hosseini S. Hamed S. Investigation of flexoelectric effect on nonlinear forced vibration of piezoelectric/functionally graded porous nanocomposite resting on viscoelastic foundation *The Journal of Strain Analysis for Engineering Design* **2020** *55*(1-2), 53–68.

[20] Ebrahimi F., Karimiasl M., Singhal A. Magneto-electro-elastic analysis of piezoelectric-flexoelectric nanobeams rested on silica aerogel foundation, *Engineering with Computers* **2021** *37*(2), 1007–1014.

[21] Abdollahi A., Arias I. Constructive and Destructive Interplay Between Piezoelectricity and Flexoelectricity in Flexural Sensors and Actuators, *J. Appl. Mech.* **2015**, *82*(12), 121003.

[22] Zeng S., Wang B.L., Wang K.F. Nonlinear vibration of piezoelectric sandwich nanoplates with functionally graded porous core with consideration of flexoelectric effect, *Composite Struct.* **2019**, *207*, 340–351.

[23] Benveniste Y. The effective conductivity of composites with imperfect thermal contact at constituent interfaces, *Int. J.Eng. Sci* **1986**, *24*,1537–1552.

[24] Benveniste Y. Effective thermal-conductivity of composites with a thermal contact resistance between the constituents-nondilute case, *J. Appl. Phys.* **1987**, *61*, 2840–2843.

[25] Javili A., Kaessmair S., Steinmann P. General imperfect interfaces, *Comput. Methods Appl. Mech. Engrg.* , **2014**, *275*, 76–97.

[26] Geymonat G., Krasucki F., Lenci S. Mathematical Analysis of a bonded joint with a soft thin adhesive, *Math. Mech. Solids*, **1999**, *16*, 201–225 (1999).

[27] Serpilli M., Lenci S. Asymptotic modelling of the linear dynamics of laminated beams *Int. J. Solids Struct.* **2012**, *49(9)*, 1147–1157.

[28] Serpilli, M., Lenci S. An overview of different asymptotic models for anisotropic three-layer plates with soft adhesive, *Int. J. Solids Struct.* **2016**, *81* 130–140.

[29] Lebon F., Rizzoni R. Asymptotic analysis of a thin interface: the case involving similar rigidity, *Int. J. Eng. Sci.* **2010**, *48*, 473–486.

[30] Lebon F., Rizzoni R. Asymptotic behavior of a hard thin linear interphase: An energy approach, *Int. J. Solids Struct.* **2011**, *48* 441–449.

[31] Rizzoni R., Dumont S., Lebon F., Sacco, E. Higher order model for soft and hard elastic interfaces, *Int. J. Solids Struct.* **2014**, *51*, 4137–4148.

[32] Dumont S., Rizzoni R., Lebon, F., Sacco E. Soft and hard interface models for bonded elements, *Composites Part B: Engineering* **2018**, *153*, 480–490.

[33] Serpilli M., Rizzoni R., Lebon F., Dumont S. An asymptotic derivation of a general imperfect interface law for linear multiphysics composites. *Int. J. Solids Struct* **2019**, *180-181*, 97–107.

[34] Dumont S., Serpilli M., Rizzoni R., Lebon, F. Numerical Validation of Multiphysic Imperfect Interfaces Models *Front. Mater.* **2020**, *158*, 1–13. doi: 10.3389/fmats.2020.00158

[35] Serpilli, M. On modeling interfaces in linear micropolar composites, *Math. Mech. Solids* **2018**, *23(4)*, 667–685.

[36] Serpilli, M. Classical and higher order interface conditions in poroelasticity, *Ann. Solid Struct. Mech.* **2019**, *11(1-2)* .

[37] Serpilli M., Dumont S., Rizzoni R., Lebon F. Interface Models in Coupled Thermoelasticity, *Technologies* **2021**, *9(1)* 17.

[38] Serpilli, M. Mathematical modeling of weak and strong piezoelectric interfaces, *J. Elasticity* **2015**, *121(2)* 235–254.

[39] Serpilli, M. Asymptotic interface models in magneto-electro-thermoelastic composites, *Meccanica* **2017**, *52(6)* 1407–1424.

[40] Serpilli M., Rizzoni R., Dumont S., Lebon F. Higher order interface conditions for piezoelectric spherical hollow composites: asymptotic approach and transfer matrix homogenization method, *Composite Struct.* **2022**, *279* 114760.

[41] Guinovart-Sanjuán D., Merodio J., López-Realpozo J.C., Vajravelu K., Rodríguez-Ramos R., Guinovart-Díaz R., Bravo-Castillero J., Sabina F.J. Asymptotic Homogenization Applied to Flexoelectric Rods, *Materials* **2019**, *12*, 232.

[42] Guinovart-Sanjuán D., Vajravelu K., Rodríguez-Ramos R., Guinovart-Díaz R., Bravo-Castillero J., Lebon F., Sabina F.J., Merodio J. Effective predictions of heterogeneous flexoelectric multilayered composite with generalized periodicity, *Int. J. Mech. Sci.* **2020**, *181*, 105755.

[43] Guinovart-Sanjuán D., Vajravelu K., Rodríguez-Ramos R., Guinovart-Díaz R., Sabina F.J., Merodio J. Simple closed-form expressions for the effective properties of multilaminated flexoelectric composites *J. Eng. Math.* **2021**, *127*(4).

[44] Barceló-Mercader J., Codony D., Fernández-Méndez S. , Arias I. Weak enforcement of interface continuity and generalized periodicity in high-order electromechanical problems, *Int. J. Numer. Methods Eng.* **2022**, *123*, 901–923.

[45] Singhal A., Sedighi H.M., Ebrahimi F., Kuznetsova I. Comparative study of the flexoelectricity effect with a highly/weakly interface in distinct piezoelectric materials (PZT-2, PZT-4, PZT-5H, $LiNbO_3$, $BaTiO_3$), *Waves in Random and Complex Media* **2021** *31*(6), 1780–1798.

[46] Nguyen B.H., Zhuang X., Rabczuk T. Numerical model for the characterization of Maxwell-Wagner relaxation in piezoelectric and flexoelectric composite material, *Comp. Struct.* **2018**, *208*,75–91.

[47] Codony D., Mocci A., Barceló-Mercader J., Arias I. Mathematical and computational modeling of flexoelectricity, , *J. Appl. Phys.* **2021**, *130*, 231102.

[48] Maranganti R., Sharma N.D., Sharma P. Electromechanical coupling in nonpiezoelectric materials due to nanoscale nonlocal size effects: Green's function solutions and embedded inclusions, *Phys. Rev. B* **2006**, *74*, 014110.

[49] Starkov A.S., Starkov I.A. Impact of the flexocaloric effect on polarization in the flexoelectric layer, *Int. J. Solids Struct.* **2016**, *82*,65–69.

[50] Ciarlet, P.G. *Mathematical Elasticity, vol. II: Theory of Plates*, North-Holland, Amsterdam, 1997.

[51] Yang W., Hu T., Liang X., Shem S., On band structures of layered phononic crystals with flexoelectricity, *Arch. Appl. Mech.* **2018**, *88*, 629–644.

[52] Tsepoura K.G., Papargyri-Beskou S., Polyzos D., Beskos E., Static and dynamic analysis of a gradient-elastic bar in tension, *Arch. Appl. Mech.* **2002** *72*, 483–497.

[53] Nirwal S., Sahu S.A., Singhal A., Baroi J. Analysis of different boundary types on wave velocity in bedded piezo-structure with flexoelectric effect, *Composites Part B* **2019**, *167*, 434–447.

[54] Singhal A., Sedighi H.A., Ebrahimi F., Kuznetsova I. Comparative study of the flexoelectricity effect with a highly/weakly interface in distinct piezoelectric materials (PZT-2, PZT-4, PZT-5H, $LiNbO_3$, $BaTiO_3$), *Waves in Random and Complex Media* **2021**, *31*(6), 1780–1798.

[55] Shu L., Wei X., Pang T., Yao X., Wang C. Symmetry of flexoelectric coefficients in crystalline medium, *J. Appl. Phys.* **2011**, *110*, 104106.